JCTC Journal of Chemical Theory and Computation

pubs.acs.org/JCTC Letter

Self-Consistent-Charge Density-Functional Tight-Binding Parameters for Modeling an All-Solid-State Lithium Battery

Rongzhi Gao, Ziyang Hu,* Jianjun Mao, Shuguang Chen, ChiYung Yam, and GuanHua Chen*

Cite This: *J. Chem. Theory Comput.* 2023, 19, 1381−1387 Read Online

ACCESS | Metrics & More | Article Recommendations | Supporting Information

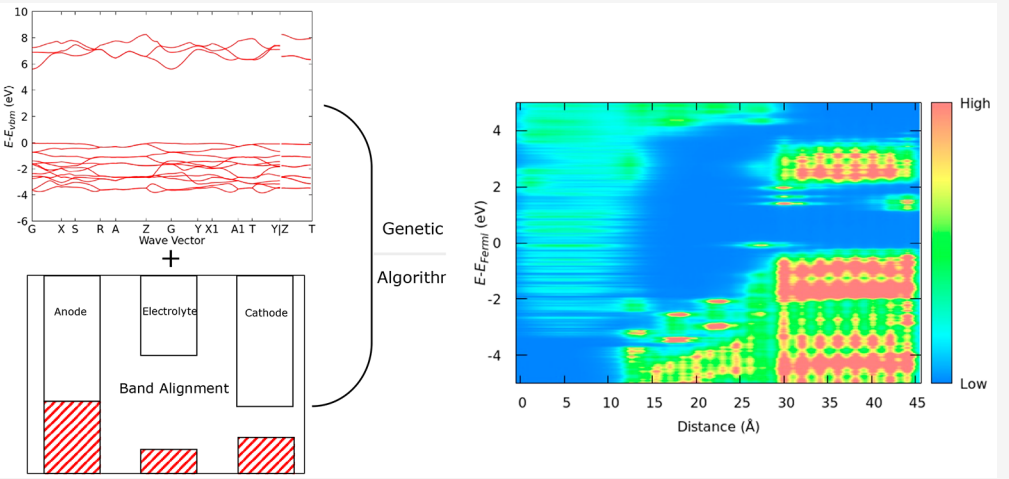

ABSTRACT: All-solid-state lithium-ion batteries have been a promising solution for next-generation energy storage due to their safety and potentially high energy density. In this work, we developed a density-functional tight-binding (DFTB) parameter set for modeling solid-state lithium batteries, focusing on the band alignment at electrolyte/electrode interfaces. Despite DFTB being widely applied in the simulation of large-scale systems, parametrization is usually done for single materials, and less attention is paid to band alignment among multiple materials. Band offsets at the electrolyte/electrode interfaces are key quantities determining the performance. Here, an automated global optimization method based on DFTB confinement potentials of all elements is developed, while the band offsets between electrodes and electrolytes are introduced as constraints during the optimization. The parameter set is applied to model an all-solid-state $Li/Li_2PO_2N/LiCoO_2$ battery, and its electronic structure shows a good agreement with that from density-functional theory (DFT) calculations.

Conventional lithium-ion batteries employ liquid electrolytes, which may cause oxidative decomposition, gas generation, and combustion at an elevated temperature.[1,2] Replacing the liquid electrolyte and separator, the solid-state electrolyte avoids using organic solvents, thus solving these safety problems.[2,3] In addition, solid electrolytes, owing to their lightness, stand out from liquid ones with extraordinary potential in increasing energy density. Currently, the energy density of lithium-ion batteries is approaching its theoretical limit and needs to catch up in meeting the demands in the fields of electric vehicles and portable electronics. Therefore, next-generation batteries with higher energy density are in strong pursuit. All-solid-state batteries are considered one of the most promising directions to achieve that goal.[4]

Given the prospects of all-solid-state batteries for various applications, it becomes necessary to fabricate them and reliably model their properties at an appropriate size and time scale. While density-functional theory[5,6] (DFT) is the most widely used electronic structure theory,[6−8] the high computational cost limits its application to relatively small systems. Alternatively, similar accuracy may be attained by applying a simplified density-functional tight-binding (DFTB) method,[9,10] which significantly reduces the computational cost using a parametrized Hamiltonian. The DFTB method exhibits a speedup of 2 orders of magnitude compared to standard DFT without a significant loss of accuracy.[11] Therefore, it serves as a computationally efficient method to facilitate the investigation of underlying processes in solid-state batteries.

Received: November 9, 2022
Published: February 22, 2023

Materials for solid-state batteries involve complex chemical compositions. Generally, a solid-state Li-ion battery comprises a cathode, an anode, and a solid electrolyte. During the discharging process, deintercalated Li-ions from the anode move across the electrolyte and intercalate into the cathode, while charging undergoes the reverse process.[12] Meanwhile, the electrolyte is responsible for transporting Li-ion and blocking electrons.[13] Therefore, at the electrolyte/electrode interfaces, the electronic structure plays a significant role in determining these devices' ion transport and performance. From the modeling perspective, an accurate description of the band alignments at these interfaces is crucial to simulate these processes in batteries. Band alignment can be calculated based on the branching point energy (BPE)[14−18] or charge neutrality level[19,20] as a common reference. In this way, energy bands of different semiconductor materials can be aligned without building a contact interface. In this work, the relative positions of the valence band maximum (VBM) and Fermi level between electrodes and electrolytes are precalculated to ensure a correct band alignment. An automated global optimization method using the multielement confinement potential is developed. The process is based on a genetic algorithm[21,22] implemented in Python to fit the electronic structure and band alignment of the electrolyte/electrode composite in all-solid-state lithium-ion batteries, which provides an automatic tool to generate DFTB parameter sets.

This letter is organized as follows. First, the DFTB method is introduced in Section I. A description of our optimization tool for parametrization follows this. A parameter set explicitly developed for the all-solid-state lithium-ion battery (Li/Li_2PO_2N/$LiCoO_2$ battery composite) is then applied to simulate the interfacial electronic properties. The calculated electronic structure reproduces the result of DFT with Perdew−Burke−Ernzerhof functional (PBE)[23] calculations. We further calculate the electrical parameters of the battery at different states of charging, and a good agreement with experimental data is achieved. Finally, we summarize this work in Section III.

I. METHODOLOGY

The DFTB method is based on the second-order expansion of the Kohn−Sham total energy[9,10,24] with respect to charge density fluctuations $\delta\rho(\boldsymbol{r})$

$$E = \sum_{i}^{\mathrm{occ}} \left\langle \psi_i \middle| -\frac{1}{2}\nabla^2 + V_{\mathrm{ext}} + V_{\mathrm{H}}[\rho_0] + V_{\mathrm{xc}}[\rho_0] \middle| \psi_i \right\rangle + \frac{1}{2}\iint' \left(\frac{\delta^2 E_{\mathrm{xc}}[\rho_0]}{\delta\rho\delta\rho'} + \frac{1}{|\boldsymbol{r}' - \boldsymbol{r}|} \right) \delta\rho\delta\rho' - \frac{1}{2}\int V_{\mathrm{H}}[\rho_0](\boldsymbol{r})\rho_0(\boldsymbol{r}) + E_{\mathrm{xc}}[\rho_0] + E_{\mathrm{ion}} - \int V_{\mathrm{xc}}[\rho_0](\boldsymbol{r})\rho_0(\boldsymbol{r}) \tag{1}$$

The first term is the band structure energy, E_{BS}, arising from a Hamiltonian built on the reference density, ρ_0. The second term, E_{SCC}, captures second-order charge fluctuations due to Coulomb and exchange-correlation interactions, which is solved self-consistently. The last line contains two-body interactions, which are collected into a single energy term, the repulsive energy, E_{rep}.

In DFTB, a minimal basis is used which contains only one radial function for each angular momentum orbital. The single-electron molecular orbital can be written as a linear combination of atomic orbitals

$$\psi_i(\boldsymbol{r}) = \sum_{\mu} c_{\mu}^{i} \varphi_{\mu}(\boldsymbol{r}) \tag{2}$$

Application of the variation principle with respect to the coefficients gives out the secular equations

$$\sum_{\nu} c_{\nu i}(h_{\mu\nu} - \varepsilon_i s_{\mu\nu}) = 0 \tag{3}$$

$$h_{\mu\nu} = h^0_{\mu\nu} + h^1_{\mu\nu}, \quad h^1_{\mu\nu} = \frac{1}{2} s_{\mu\nu} \sum_{I} (\gamma_{AI} + \gamma_{BI})\Delta q_I, \quad \mu \in A, \nu \in B \tag{4}$$

where $h_{\mu\nu}$ is the elements of the Hamiltonian; h^0 and s are the parametrized Hamiltonian and overlap matrices as described in the next section; A, B, and I label atom indices in the system; and h^1 reflects the electrostatic potential between atom A and B due to charge fluctuations. The γ matrix is determined by the types and distance between atoms A/B and I. Eq 3 must be solved iteratively because the Hamiltonian matrix elements depend on the Mulliken charges,[25] which in turn depend on the molecular orbital coefficients, $c_{\nu i}$.

To obtain the matrices h^0 and s, the atomic orbitals are first solved for pseudoatoms, which are determined from an atomic DFT calculation with an artificial confinement potential

$$\left[-\frac{1}{2}\nabla^2 - \frac{Z}{r} + V_{\mathrm{H}}(r) + V_{\mathrm{xc}}(r) + \left(\frac{r}{r_0}\right)^p \right] \varphi_i = \varepsilon_i \varphi_i \tag{5}$$

The additional confinement potential compresses the atomic orbitals to represent the chemical environment when bonded in a solid. The confinement potential is characterized by the confinement radius r_0 and the exponent p which are per chemical element.

Using the orbitals of the pseudoatom, overlap matrix elements can be calculated

$$s_{\mu\nu} = \int \varphi_{\mu}(\boldsymbol{r})^* \varphi_{\nu}(\boldsymbol{r})\, \mathrm{d}\boldsymbol{r} \tag{6}$$

Similarly, the Hamiltonian matrix elements are obtained as

$$h^0_{\mu\nu} = \int \varphi_{\mu}(\boldsymbol{r})^* \left[-\frac{1}{2}\nabla^2 + V_{\mathrm{ext}}(\boldsymbol{r}) + V_{\mathrm{H}}[\rho_0](\boldsymbol{r}) + V_{\mathrm{xc}}[\rho_0](\boldsymbol{r}) \right] \varphi_{\nu}(r)\, \mathrm{d}\boldsymbol{r} = \int \varphi_{\mu}(\boldsymbol{r})^* \left[-\frac{1}{2}\nabla^2 + V_{\mathrm{eff}}[\rho_0] \right] \varphi_{\nu}(\boldsymbol{r})\, \mathrm{d}\boldsymbol{r} \tag{7}$$

where $V_{\mathrm{eff}}[\rho_0]$ is the effective potential evaluated at the neutral density ρ_0 of the system. Here, the one-center approximation is adopted for the diagonal elements, $h_{\mu\mu} = \varepsilon_{\mu}$, where ε_{μ} is the eigenenergy of free atoms. For off-diagonal elements, three-center and four-center terms are ignored which leads to

$$V_{\mathrm{eff}}[\rho_0](\boldsymbol{r}) \approx V_A[\rho_{0,A}](\boldsymbol{r}) + V_B[\rho_{0,B}](\boldsymbol{r}) \tag{8a}$$

or

$$V_{\mathrm{eff}}[\rho_0](\boldsymbol{r}) = V_{\mathrm{eff}}[\rho_0^A + \rho_0^B] \tag{8b}$$

where $V_A[\rho_{0,A}](\boldsymbol{r})$ is the Kohn−Sham potential with the density of a neutral atom. The effective potential can be approximated as a sum of the effective potentials of two atoms,[24] which is called *potential superposition* as in eq 8a. The effective potential can also be calculated from the sum of electron density, called *density superpositions* as in eq 8b.[10] Eqs 6 and 7 are integrated numerically to obtain the required

https://doi.org/10.1021/acs.jctc.2c01115
J. Chem. Theory Comput. 2023, 19, 1381−1387

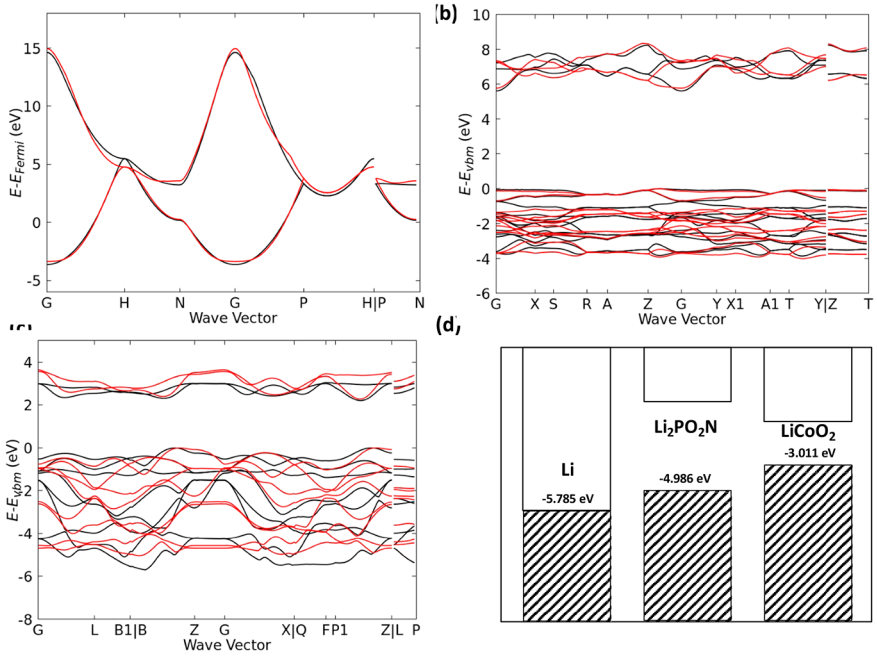

Figure 1. Band structure of (a) Im$\bar{3}$m-lithium, (b) Cmc2$_1$-Li_2PO_2N, and (c) R$\bar{3}$m-$LiCoO_2$. Black lines: DFT and red lines: DFTB results. (d) Relative energy levels of the battery composites. Shaded area: occupied orbitals. Here, the VBM of $LiCoO_2$ is higher than the Fermi level of Li, and this false alignment fails to describe the electrochemical properties of the battery.

Slater-Koster integrals for all orbital pairs. This is done for a set of distances, and the integrals are stored in a table.

The optimization process is done using the genetic algorithm originated from simulations of biological systems.[21,26] In the optimization process, we used an initial population of 50 and a mutation probability of 0.5% to vary the confinement radii r_0 and exponents p of Li, P, O, N, and Co. During the potential superposition optimization process, the density compression and wave function compression radii and exponents are all varied independently to get better band structures. Hubbard values can be obtained as the partial derivative of the single atomic orbital energy with respect to the orbital occupancy number.[27] And on-site energies, i.e., the orbital energies, are calculated by Slater-type basis functions with proper orbital exponents. The Hubbard and on-site values obtained by the basis functions we chose are almost consistent with the results obtained by T. Heine et al.[28] In general, Hubbard values of the highest occupied shell are chosen. However, for P, we found the electronic structure of LiPON is significantly improved if the Hubbard value of the d shell is used, instead of the p shell. This can be attributed to the fact that d orbitals of P are partially occupied in LiPON. Eigenvalues at high symmetry points are chosen, and their root mean square differences (RMSDs) compared to DFT results are evaluated during the genetic algorithm process. A loss function is calculated based on the RMSD and their corresponding weights. Parameters in the confinement potential of eq 5 are then updated based on the loss function, and the process is repeated until the error is lower than a preset value. All self-consistent-charge DFTB[10] calculations are done using DFTB+,[29] while DFT calculations are done using the *Vienna Ab initio Simulation Package* (VASP).[30] The VASP calculations are performed with the PBE+U[31,32] ($U - J$ = 3.3 eV for cobalt) functional and a 520 eV energy cutoff. We used the VASPKIT[33] code for postprocessing slab calculations of VASP and the DensityTool package[34] to compute the local density of states from the projected density of states output by VASP. For DFTB+, the PBE functional is used to generate Slater-Koster files. The zeroth-order regular approximation (ZORA)[35] and DFTB+U[36] fully localized limit function are applied to cobalt ($U - J$ = 3.3 eV), while the relativistic effects of VASP are included in the pseudopotential. The DFT band structure of $LiCoO_2$ without +U correction is difficult to fit, so we use the DFTB+U method to fit the DFT+U results with the same $U - J$ value.

II. RESULTS AND DISCUSSION

In this work, Li metal is chosen as the anode, while Li_2PO_2N (denoted as LiPON) and $LiCoO_2$ are used as the electrolyte and cathode, respectively. As the first step, the electronic structure of lithium metal is optimized. The body-centered cubic (bcc) structure is the most stable form for lithium metal at ambient conditions and is therefore chosen as the reference structure (Im$\bar{3}$m-Li). We choose four atomic orbitals to represent Li, with an electronic configuration of $2s^1 2p^0$, and use different confinement radii for different angular momenta. For the bcc lithium metal, we found that potential superposition is better than density superposition in terms of the resulting band structure. Since we are interested in the performance of batteries, the bands within the open-circuit voltage of the battery are most relevant. Therefore, the frontier orbitals within −5 and 5 eV with respect to the Fermi level are optimized against DFT/PBE+U results. The result of the optimization is reported in Figure 1(a), which shows a good agreement compared with the DFT band structure. The space group of LiPON is Cmc2$_1$, while that of $LiCoO_2$ is R$\bar{3}$m. All these structures are obtained from MaterialsProject[37] and further optimized using VASP. With the optimized Li parameters, we proceed with the parametrization for both electrolyte and cathode materials. The confinement potentials of N, O, P, and Co are varied. To achieve a better agreement of bandgaps, 10 times larger weights are given for the first

https://doi.org/10.1021/acs.jctc.2c01115
J. Chem. Theory Comput. 2023, 19, 1381−1387

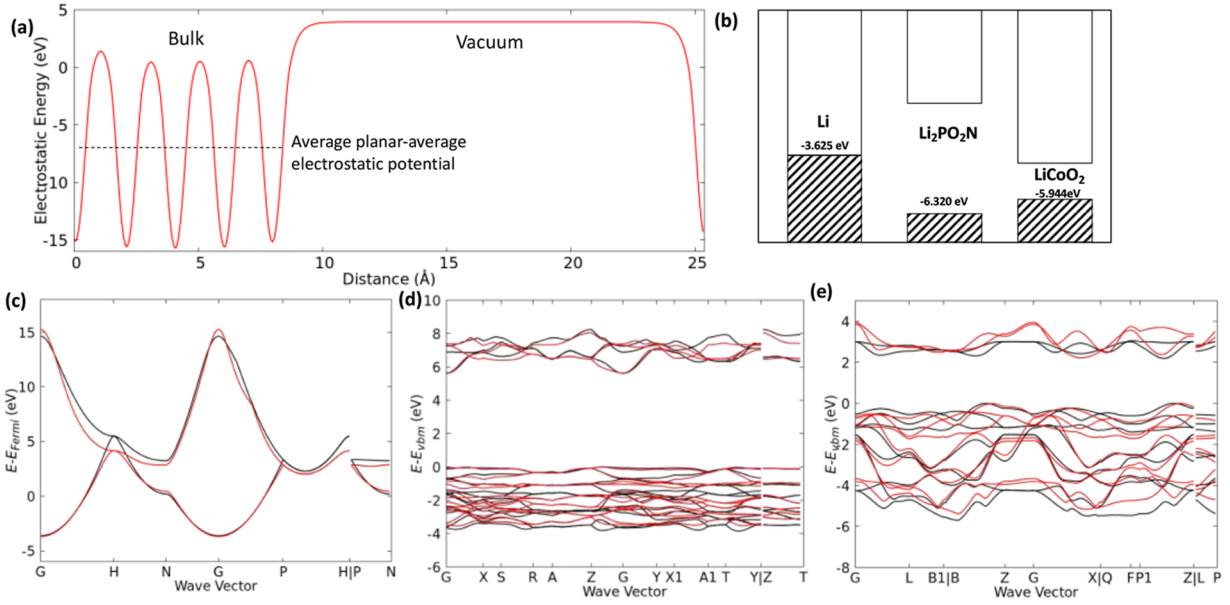

Figure 2. (a) Electrostatic potential curve of $LiCoO_2$ (about a 10-Å bulk and 15-Å vacuum) to obtain the absolute energy level of the DFT. (b) Relative energy levels of the battery composites. Shaded area: occupied orbitals. Band structures of (c) Li, (d) LiPON, and (e) $LiCoO_2$ after band alignment. Black lines: DFT and red lines: DFTB results.

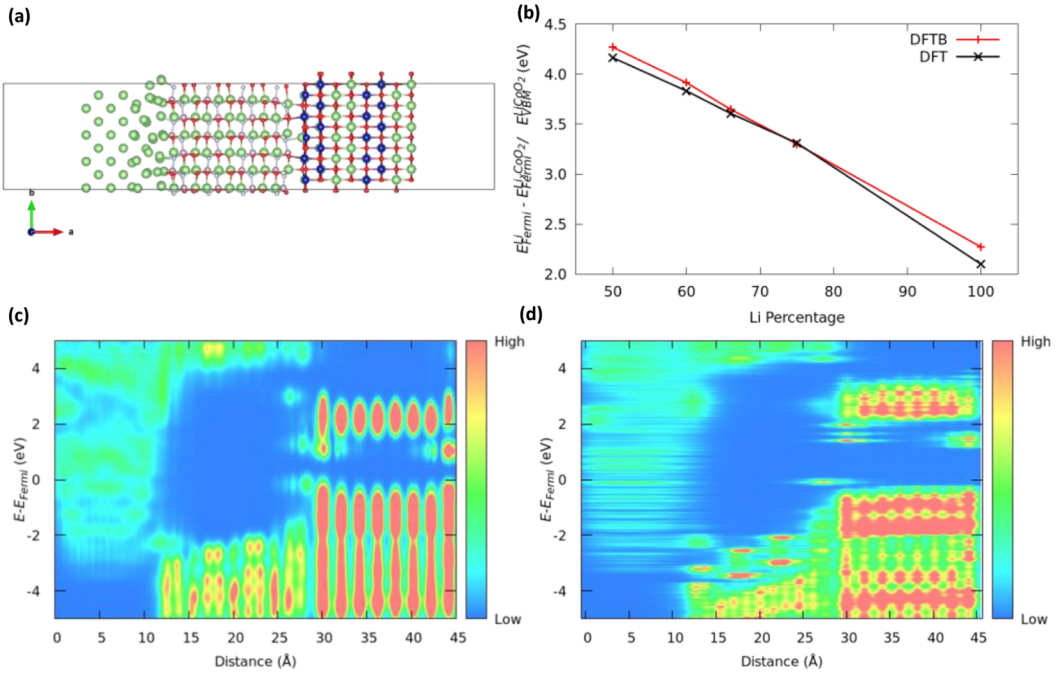

Figure 3. (a) Atomic structure of a model battery composite, including the anode (Li), electrolyte (Li_2PO_2N), and cathode ($LiCoO_2$). (b) Fermi levels or the Fermi level/VBM difference between the anode and cathode at different Li concentrations. Black line: DFT and red line: DFTB. Local density of states of the model was calculated by (c) DFT+U and (d) DFTB+U.

conduction band energies when we evaluate the loss function. The resulting band structures for the two materials are plotted in Figure 1(b)-(c). Overall, the DFTB calculation reproduces the PBE band structures, particularly for bands that are close to Fermi energy for both materials. For bands away from the bandgap, DFTB results still quantitatively agree with PBE.

In this way, the optimization is done separately for each material without considering band alignments between them. As discussed above, although electronic properties are obtained individually, the band alignments between electrolytes and electrodes are key quantities to ensure accurate descriptions of the underlying processes in batteries. We examine the relative energies between the three materials in Figure 1(d). The VBM of the cathode material is higher than the Fermi level of the anode material, which fails to describe electrochemical processes in battery systems. The results reveal that band offsets must be considered explicitly during the DFTB optimization of the electronic part. To determine the relative

https://doi.org/10.1021/acs.jctc.2c01115
J. Chem. Theory Comput. 2023, 19, 1381−1387

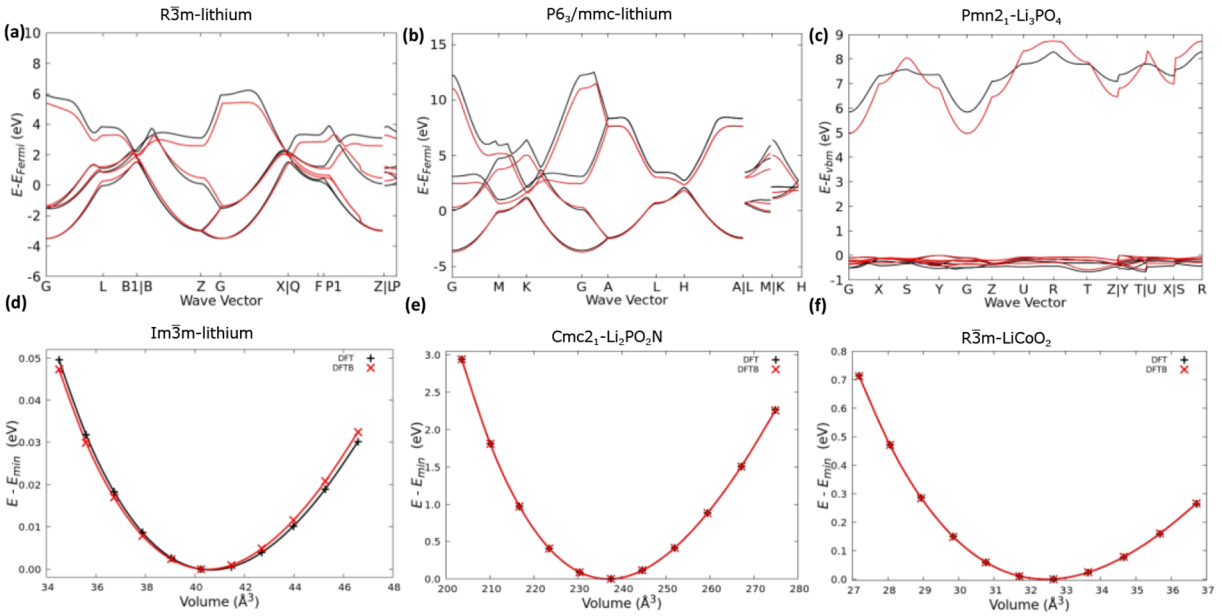

Figure 4. Band structures of (a) R$\bar{3}$m-lithium, (b) *P*6$_3$/*mmc*-lithium, and (c) Pmn2$_1$-Li$_3$PO$_4$ for transferability of the band alignment parameter set. Black lines: DFT and red lines: DFTB results. Equation of state curves of (d) Im$\bar{3}$m-lithium, (e) Cmc2$_1$-Li$_2$PO$_2$N, and (f) R3m-LiCoO$_2$ for DFTB repulsive part fitting. Black curves: DFT and red curves: DFTB results.

energy levels between electrolyte and electrodes, we calculate the average bulk electrostatic potential with respect to the vacuum level for each material using VASP as shown in Figure 2(a). Unit cells of Li, LiPON, and LiCoO$_2$ were calculated to obtain the Fermi level of Li, the VBM of LiPON and LiCoO$_2$, and average bulk electrostatic potentials using VASP. In addition, slab models of Li with the (1, 0, 0) surface, LiPON with the (1, −1, 0) surface, and LiCoO$_2$ with the (1, 0, 4) surface were also calculated. About 10 Å of Li, LiPON, or the LiCoO$_2$ bulk structure and 15 Å of the vacuum region were used to get the average bulk electrostatic potentials and vacuum potentials. We can thus approximately compute the Fermi level/VBM relative to the vacuum. For DFTB, since the vacuum level is 0 eV (see SI Part 4), the calculated energy levels of each material are already with reference to the vacuum level. For the composite system, a potential superposition scheme is used in the pseudoatom calculations. In addition, we found that if we used the preoptimized density superposition parameter of Li−Li during the GA process, the electronic structure of LiPON and band alignments would become better (see SI Part 3). Thus, the parameter of Li−Li is replaced by the preoptimized density superposition during one band alignment optimization (i.e., Li−Li integrals with density superposition, Li-X and X-Li integrals with potential superposition). Consequently, all three materials are optimized again simultaneously, where the band alignments between them are explicitly included in the loss function. Considering the band offsets between each material, the optimized electronic structures for Li, Li$_2$PO$_2$N, and LiCoO$_2$ are plotted in Figure 2. As compared to the band structures in Figure 1, the overall agreement with DFT results is preserved. A notable exception is the dispersion of the conduction band in LiCoO$_2$ and LiPON due to the extra constraints imposed. The parameter set is then applied to simulate a model battery system, as shown in Figure 3(a), rendered using VESTA.[38] The battery system consists of the anode Li, electrolyte LiPON, and cathode LiCoO$_2$. All directions are periodic, while the *a* direction has 10-Å vacuums on both sides.

The electronic structure of the Li/Li$_2$PO$_2$N/LiCoO$_2$ composite is simulated with DFTB as implemented in LODESTAR.[39] The local density of states (LDOS), i.e., the projected density of states along the ion transport direction in real space, is plotted in Figure 3(d). Similarly, the same model is calculated using DFT for comparison, and the resulting LDOS is reported in Figure 3(c). As shown in Figure 3(d), the band gaps of LiPON and LiCoO$_2$ are 5.8 and 1.1 eV, respectively, which are in good agreement with that of DFT (5.8 and 1.0 eV). More importantly, the composite demonstrates a correct energy alignment between electrodes and electrolytes. DFTB's band offsets between Li/LiPON and LiPON/LiCoO$_2$ are 2.69 and 0.38 eV, respectively, while DFT's band offsets are 2.40 and 0.43 eV, respectively. When the battery is charged and discharged, the relative energy level positions of different lithium-ion concentrations in the cathode play a key role in determining the performance of the battery.[7] We prepared many structures with different Li concentrations by randomly removing lithium atoms in a supercell of LiCoO$_2$. Here, we generate Li$_{0.5}$CoO$_2$, Li$_{0.6}$CoO$_2$, Li$_{0.667}$CoO$_2$, and Li$_{0.75}$CoO$_2$. The VASP (PBE+U) geometry optimizations are performed on these structures, the single point energies are calculated, and the lowest energy structures of LiCoO$_2$ with different Li concentrations are selected. Figure 3(b) shows the comparison of the Fermi level difference between Li and Li$_x$CoO$_2$ for PBE and DFTB at different *x* values[40] and the Fermi level/VBM difference between Li and LiCoO$_2$. The Fermi level or Fermi level/VBM difference is a key quantity that determines the battery's open circuit voltage. From Figure 3(b), it can be clearly seen that the current parameter set correctly predicts the electrical characteristics at different battery charge states. This further demonstrates the applicability of the present parameter set to simulate the all-solid-state lithium battery.[7,40]

https://doi.org/10.1021/acs.jctc.2c01115
J. Chem. Theory Comput. 2023, 19, 1381−1387

One critical issue of the DFTB method is the transferability of its parameters. While the band alignment of the Li/Li_2PO_2N/$LiCoO_2$ composite is enforced, the transferability of the current parameter set to other materials is questionable. Thus, we calculate the electronic structures of different compounds to examine the transferability of the current parameter set. Li's parameters in our band alignment parameter set are optimized with Im$\bar{3}$m-lithium. In the case of R$\bar{3}$m-lithium and $P6_3/mmc$-lithium (see Figure 4(a)-(b)), the DFTB calculation essentially reproduces the DFT/PBE band structures. In addition, the transferability of the Li_2PO_2N parameters is examined by calculating $Pmm2_1$-lithium phosphate. The results also show the excellent agreement of the electronic structure compared to DFT/PBE (Figure 4(c)). On the other hand, the agreement of the Fermi levels of Li_xCoO_2 with different lithium concentrations for PBE and DFTB also indicates that the parameters have good transferability between different lithium cobalt oxide materials (Figure 3(b)). Overall, the agreements between electronic structures for these compounds, obtained within DFTB and PBE+U approaches, are reasonably good, demonstrating the transferability of the method we developed.

Besides the DFT-accuracy electronic part in our band alignment parameters set, we also fitted the repulsive potentials. The repulsive potentials are obtained by fitting the DFT's equation of state curves of Li, LiPON, and $LiCoO_2$ (VASP/PBE+U calculation). The Li's equation of state curve was fitted first in Im$\bar{3}$m-Li (see Figure 4(d)), and the fitted repulsive parameters of Li−Li were used in fitting the other LiPON's repulsive parameters (see Figure 4(e)). Repulsive parameters of Li−Li, Li−O, and O−O obtained by Li and LiPON were then applied to fit the $LiCoO_2$'s (Co−Li, Co−O, and Co−Co) repulsive parameters (see Figure 4(f)). The DFT and DFTB equation of state curves are aligned with their minimum energies (E_{min}), respectively. Bulk moduli are calculated by DFT (Li: 13.625 GPa, LiPON: 154.617 GPa, and $LiCoO_2$: 193.046 GPa) and DFTB (Li: 13.765 GPa, LiPON: 154.604 GPa, and $LiCoO_2$: 193.240 GPa), respectively. The excellent agreement of the equation of state curves and bulk modulus shows that the obtained band alignment electronic parameter set could generate satisfactory repulsive parameters.

III. CONCLUSIONS AND PROSPECTS

We proposed a DFTB parametrization scheme for the band alignment of an interfacial system. In the optimization process, we only need to perform a first-principles calculation to obtain the standard band structure or use experimental data as a reference to obtain the more accurate electronic structure of DFTB. We succeeded in developing a set of DFTB electronic structure parameters for a typical all-solid-state lithium-ion battery system (Li/Li_2PO_2N/$LiCoO_2$). This set of parameters considers the band structure of the three crystals and the band alignments among them. The parameters generated by this method are transferable for the systems made of the same elements and the Fermi levels of Li_xCoO_2 which represent different charge and discharge states in the batteries. In the future, we will focus on the complex battery system which enables the molecular dynamics simulation based on this set of DFTB parameters.

■ ASSOCIATED CONTENT

Data Availability Statement

Slater-Koster files including the repulsive part are available from the corresponding authors upon reasonable request.

Supporting Information

The Supporting Information is available free of charge at https://pubs.acs.org/doi/10.1021/acs.jctc.2c01115.

SCC-DFTB electronic parameters optimized in this study (PDF)

■ AUTHOR INFORMATION

Corresponding Authors

Ziyang Hu − *Department of Chemistry, The University of Hong Kong, Hong Kong SAR 999077, China; Hong Kong Quantum AI Lab Limited, Hong Kong SAR 999077, China;* orcid.org/0000-0002-7693-5457; Email: hzy@yangtze.hku.hk

GuanHua Chen − *Department of Chemistry, The University of Hong Kong, Hong Kong SAR 999077, China; Hong Kong Quantum AI Lab Limited, Hong Kong SAR 999077, China;* orcid.org/0000-0001-5015-0902; Email: ghc@everest.hku.hk

Authors

Rongzhi Gao − *Department of Chemistry, The University of Hong Kong, Hong Kong SAR 999077, China;* orcid.org/0000-0001-7520-0347

Jianjun Mao − *Hong Kong Quantum AI Lab Limited, Hong Kong SAR 999077, China;* orcid.org/0000-0003-2265-9685

Shuguang Chen − *Department of Chemistry, The University of Hong Kong, Hong Kong SAR 999077, China; Hong Kong Quantum AI Lab Limited, Hong Kong SAR 999077, China*

ChiYung Yam − *Hong Kong Quantum AI Lab Limited, Hong Kong SAR 999077, China; Shenzhen Institute for Advanced Study, University of Electronic Science and Technology of China, Shenzhen 518000, China*

Complete contact information is available at: https://pubs.acs.org/10.1021/acs.jctc.2c01115

Notes

The authors declare no competing financial interest.

■ ACKNOWLEDGMENTS

The financial support from the RGC General Research Fund (Grant No. 17309620), Hong Kong Quantum AI Lab Limited, Air @ InnoHK of Hong Kong Government, the Guangdong Shenzhen Joint Key Fund (Grant No. 2019B1515120045), and the National Natural Science Foundation of China (Grant No. 22073007) are gratefully acknowledged.

■ REFERENCES

(1) Chombo, P. V.; Laoonual, Y. A review of safety strategies of a Li-ion battery. *J. Power Sources* **2020**, *478*, 228649.

(2) Gao, Z.; Sun, H.; Fu, L.; Ye, F.; Zhang, Y.; Luo, W.; Huang, Y. Promises, Challenges, and Recent Progress of Inorganic Solid-State Electrolytes for All-Solid-State Lithium Batteries. *Adv. Mater.* **2018**, *30* (17), 1705702.

(3) Randau, S.; Weber, D. A.; Kötz, O.; Koerver, R.; Braun, P.; Weber, A.; Ivers-Tiffée, E.; Adermann, T.; Kulisch, J.; Zeier, W. G.; et al. Benchmarking the performance of all-solid-state lithium batteries. *Nature Energy* **2020**, *5* (3), 259−270.

(4) Wu, F.; Maier, J.; Yu, Y. Guidelines and trends for next-generation rechargeable lithium and lithium-ion batteries. *Chem. Soc. Rev.* **2020**, *49* (5), 1569−1614.
(5) Hohenberg, P.; Kohn, W. Inhomogeneous Electron Gas. *Phys. Rev.* **1964**, *136* (3B), B864−B871.
(6) Kohn, W.; Sham, L. J. Self-Consistent Equations Including Exchange and Correlation Effects. *Phys. Rev.* **1965**, *140* (4A), A1133−A1138.
(7) Swift, M. W.; Qi, Y. First-Principles Prediction of Potentials and Space-Charge Layers in All-Solid-State Batteries. *Phys. Rev. Lett.* **2019**, *122* (16), 167701.
(8) Jalem, R.; Tateyama, Y.; Takada, K.; Nakayama, M. First-Principles DFT Study on Inverse Ruddlesden-Popper Tetragonal Compounds as Solid Electrolytes for All-Solid-State Li+-Ion Batteries. *Chem. Mater.* **2021**, *33* (15), 5859−5871.
(9) Porezag, D.; Frauenheim, T.; Köhler, T.; Seifert, G.; Kaschner, R. Construction of tight-binding-like potentials on the basis of density-functional theory: Application to carbon. *Phys. Rev. B* **1995**, *51* (19), 12947−12957.
(10) Elstner, M.; Porezag, D.; Jungnickel, G.; Elsner, J.; Haugk, M.; Frauenheim, T.; Suhai, S.; Seifert, G. Self-consistent-charge density-functional tight-binding method for simulations of complex materials properties. *Phys. Rev. B* **1998**, *58* (11), 7260−7268.
(11) Elstner, M.; Frauenheim, T.; Suhai, S. An approximate DFT method for QM/MM simulations of biological structures and processes. *Journal of Molecular Structure: THEOCHEM* **2003**, *632* (1), 29−41.
(12) Raijmakers, L. H. J.; Danilov, D. L.; Eichel, R. A.; Notten, P. H. L. An advanced all-solid-state Li-ion battery model. *Electrochim. Acta* **2020**, *330*, 135147.
(13) Robertson, J. Band offsets, Schottky barrier heights, and their effects on electronic devices. *Journal of Vacuum Science & Technology A* **2013**, *31* (5), 050821.
(14) Kohn, W. Analytic Properties of Bloch Waves and Wannier Functions. *Phys. Rev.* **1959**, *115* (4), 809−821.
(15) Rehr, J. J.; Kohn, W. Impurity states between two bands. *Phys. Rev. B* **1974**, *9* (4), 1981−1983.
(16) Tersoff, J. Schottky Barrier Heights and the Continuum of Gap States. *Phys. Rev. Lett.* **1984**, *52* (12), 1054−1055.
(17) Schleife, A.; Fuchs, F.; Rödl, C.; Furthmüller, J.; Bechstedt, F. Branch-point energies and band discontinuities of III-nitrides and III-/II-oxides from quasiparticle band-structure calculations. *Appl. Phys. Lett.* **2009**, *94* (1), 012104.
(18) Deák, P.; Aradi, B.; Frauenheim, T. Band Lineup and Charge Carrier Separation in Mixed Rutile-Anatase Systems. *J. Phys. Chem. C* **2011**, *115* (8), 3443−3446.
(19) Gallinaro, G.; Marinelli, M.; Morpurgo, G. Electric Neutrality of Matter. *Phys. Rev. Lett.* **1977**, *38* (22), 1255−1258.
(20) Flores, F.; Tejedor, C. Energy barriers and interface states at heterojunctions. *Journal of Physics C: Solid State Physics* **1979**, *12* (4), 731−749.
(21) Whitley, D. A genetic algorithm tutorial. *Statistics and Computing* **1994**, *4* (2), 65−85.
(22) Chollet, F. *Deep Learning with Python*, 2nd ed.; Manning: 2021.
(23) Perdew, J. P.; Burke, K.; Ernzerhof, M. Generalized Gradient Approximation Made Simple. *Phys. Rev. Lett.* **1996**, *77* (18), 3865−3868.
(24) Koskinen, P.; Mäkinen, V. Density-functional tight-binding for beginners. *Comput. Mater. Sci.* **2009**, *47* (1), 237−253.
(25) Hou, G.; Zhu, X.; Cui, Q. An Implicit Solvent Model for SCC-DFTB with Charge-Dependent Radii. *J. Chem. Theory Comput.* **2010**, *6* (8), 2303−2314.
(26) Bäck, T.; Schwefel, H. An Overview of Evolutionary Algorithms for Parameter Optimization. *Evolutionary Computation* **1993**, *1* (1), 1−23.
(27) Janak, J. F. Proof that $\partial E/\partial n_i = \varepsilon$ in density-functional theory. *Phys. Rev. B* **1978**, *18* (12), 7165−7168.
(28) Wahiduzzaman, M.; Oliveira, A. F.; Philipsen, P.; Zhechkov, L.; van Lenthe, E.; Witek, H. A.; Heine, T. DFTB Parameters for the Periodic Table: Part 1, Electronic Structure. *J. Chem. Theory Comput.* **2013**, *9* (9), 4006−4017.
(29) Hourahine, B.; Aradi, B.; Blum, V.; Bonafé, F.; Buccheri, A.; Camacho, C.; Cevallos, C.; Deshaye, M. Y.; Dumitrică, T.; Dominguez, A.; et al. DFTB+, a software package for efficient approximate density functional theory based atomistic simulations. *J. Chem. Phys.* **2020**, *152* (12), 124101.
(30) Kresse, G.; Furthmüller, J. Efficiency of ab-initio total energy calculations for metals and semiconductors using a plane-wave basis set. *Comput. Mater. Sci.* **1996**, *6* (1), 15−50.
(31) He, Q.; Yu, B.; Li, Z.; Zhao, Y. Density Functional Theory for Battery Materials. *ENERGY & ENVIRONMENTAL MATERIALS* **2019**, *2* (4), 264−279.
(32) Dudarev, S. L.; Botton, G. A.; Savrasov, S. Y.; Humphreys, C. J.; Sutton, A. P. Electron-energy-loss spectra and the structural stability of nickel oxide: An LSDA+U study. *Phys. Rev. B* **1998**, *57*, 1505.
(33) Wang, V.; Xu, N.; Liu, J.-C.; Tang, G.; Geng, W.-T. VASPKIT: A user-friendly interface facilitating high-throughput computing and analysis using VASP code. *Comput. Phys. Commun.* **2021**, *267*, 108033.
(34) Lodeiro, L.; Rauch, T. DensityTool: A post-processing tool for space- and spin-resolved density of states from VASP. *Comput. Phys. Commun.* **2022**, *277*, 108384.
(35) Lenthe, E. v.; Baerends, E. J.; Snijders, J. G. Relativistic regular two-component Hamiltonians. *J. Chem. Phys.* **1993**, *99* (6), 4597−4610.
(36) Hourahine, B.; Sanna, S.; Aradi, B.; Köhler, C.; Niehaus, T.; Frauenheim, T. Self-Interaction and Strong Correlation in DFTB. *J. Phys. Chem. A* **2007**, *111* (26), 5671−5677.
(37) Jain, A.; Ong, S. P.; Hautier, G.; Chen, W.; Richards, W. D.; Dacek, S.; Cholia, S.; Gunter, D.; Skinner, D.; Ceder, G.; et al. Commentary: The Materials Project: A materials genome approach to accelerating materials innovation. *APL Materials* **2013**, *1* (1), 011002.
(38) Momma, K.; Izumi, F. VESTA 3 for three-dimensional visualization of crystal, volumetric and morphology data. *J. Appl. Crystallogr.* **2011**, *44* (6), 1272−1276.
(39) Yam, C.; Yokojima, S.; Chen, G. Linear-scaling time-dependent density-functional theory. *Phys. Rev. B* **2003**, *68* (15), 153105.
(40) Schwöbel, A.; Jaegermann, W.; Hausbrand, R. Interfacial energy level alignment and energy level diagrams for all-solid Li-ion cells: Impact of Li-ion transfer and double layer formation. *Solid State Ionics* **2016**, *288*, 224−228.

https://doi.org/10.1021/acs.jctc.2c01115
J. Chem. Theory Comput. 2023, 19, 1381−1387